WIND ENERGY
Wind Energ. 2012; **15**:699–715
Published online 3 October 2011 in Wiley Online Library (wileyonlinelibrary.com). DOI: 10.1002/we.499

RESEARCH ARTICLE

Generating wind time series as a hybrid of measured and simulated data

Stephen Rose and Jay Apt

Carnegie Mellon Electricity Industry Center, Carnegie Mellon University, Pittsburgh, Pennsylvania 15213, USA

ABSTRACT

Certain applications, such as analysing the effect of a wind farm on grid frequency regulation, require several years of wind power data measured at intervals of a few seconds. We have developed a method to generate days to years of non-stationary wind speed time series sampled at high rates by combining measured and simulated data. Measured wind speed data, typically 10–15 min averages, capture the non-stationary characteristics of wind speed variation: diurnal variations, the passing of weather fronts, and seasonal variations. Simulated wind speed data, generated from spectral models, add realistic turbulence between the empirical data. The wind speed time series generated with this method agree very well with measured time series, both qualitatively and quantitatively. The power output of a wind turbine simulated with wind data generated by this method demonstrates energy production, ramp rates and reserve requirements that closely match the power output of a turbine simulated turbine with measured wind data. Copyright © 2011 John Wiley & Sons, Ltd.

KEYWORDS

wind speed time series; non-stationary simulation; power fluctuation

Correspondence

Stephen Rose, Carnegie Mellon Electricity Industry Center, Carnegie Mellon University, Pittsburgh, Pennsylvania 15213, USA.
E-mail: srose@cmu.edu

Received 9 July 2010; Revised 17 June 2011; Accepted 20 June 2011

1. INTRODUCTION

Planning for frequency control in a power system with significant amounts of wind power requires both high-frequency data (∼1 Hz) to capture fast changes in power output and long periods of data to capture diurnal and seasonal variations. Similarly, simulating the fatigue life of wind turbine mechanical components requires high-frequency data to capture the dynamic effects of control system actions but long periods of data to compile statistical data to more accurately estimate lifetimes. In both cases, large amounts of data are needed to design systems that are neither overly conservative and inefficient nor unreliable.

Long wind speed data sets sampled at high rates are often difficult to obtain. Empirical data are often sampled at too slow a rate, in the wrong location or at the wrong height. Government meteorological services record many years of wind speed data, but these are typically sampled at slow rates (2 min moving average in the USA) with low amplitude resolution (1 knot, 0.51 m s^{-1}, in the USA)[1] and at locations that are not valuable for wind power development. Wind farm developers collect several years of data at potential wind power sites, but they typically record 10–15 min average values that are sufficient to estimate only long-term power production. Special scientific campaigns sometimes collect weeks to years of high-frequency data, but there are few of them because they are expensive to set up and maintain. The measurement instruments on a wind turbine are one of the best sources of this type of data, but the measurements can be confounded by the effects of the turbine and other turbines nearby, and data are frequently not archived at high temporal resolution.

Simulated wind speed data can be created at very high sampling rates, in any location, and at any height desired. However, simulation of periods longer than a few hours is difficult because wind speed variations are non-stationary processes: their statistical properties change over time. Those properties change with time of day, with the passing of weather fronts and with the seasons. Most methods for simulating long periods of wind speed data use separate models for the non-stationary variations over longer periods (e.g. hours to months) and the stationary variations over shorter periods (e.g. seconds to minutes).

Copyright © 2011 John Wiley & Sons, Ltd.

Previous authors have proposed a variety of methods for simulating non-stationary wind speed time series longer than a few hours.[2] The simulation methods divide the variations into high-frequency (periods less than approximately 15 min) and low-frequency (periods greater than 15 min) ranges. One method, which we will refer to as the 'spectral method', joins together separate spectral models for the high-frequency and low-frequency ranges in the frequency domain[3,4] and generates time series using the Veers method.[5] The other class of methods, which we will refer to as the 'parametric method', models the high-frequency range using a spectral model and the low-frequency range using a probability distribution.[6–8] Short periods (∼10 min) of high-frequency data are generated using the Veers method, blended together and then superimposed on low-frequency time-series data. Most authors blend together the short time series of high-frequency data using a window function such as the Hann function that reduces leakage of energy outside the range of simulated,[6,9] but one author concatenates together the high-frequency time series without any windowing because discontinuities are smaller than the largest sample-to-sample variations in the blocks of simulated.[7]

Both methods of modeling the low-frequency, non-stationary variations in wind speed are inadequate for certain types of power system planning and simulation because their simulations are not indexed to time of day and time of year. For example, the spectral and parametric methods can generate long time series that contain a certain level of wind speed variance with a given probability, but those methods cannot model what time of day or time of year that level of variance is likely to occur. Electrical power demand is a relatively predictable function of time of day and time of year, so wind simulations must correctly model wind properties as a function of time. Nielsen addresses this problem in a non-stationary simulation of a wind front passage by specifying the statistical properties of wind turbulence at certain reference states, using Veers method to simulate stationary turbulence at those reference states, and then interpolating between the stationary simulations with Bezier curves fit to the reference states.[10]

Our work addresses and solves the problem of correctly placing events in time by creating 'hybrid' wind speed time series that combine measured low-frequency wind speed data with simulated high-frequency data. This hybrid method is similar to the parametric methods described previously, especially Nielsen,[10] but the hybrid method uses low-frequency measured wind speed data instead of the low-frequency data generated by parametric methods and low-pass filtering of the measured data instead of windowing or interpolation. Low-frequency measured wind data are available from meteorological stations and meteorological towers at wind farms. Low-frequency wind speed data are also available from mesoscale simulations, but users should be very careful to understand the limitations of particular mesoscale models and the spatial and time resolutions of the data they generate.

Our work also improves on the procedure used in the parametric methods by filtering the low-frequency data to remove noise that leaks into the high-frequency region. This filtering fixes the problem of spurious low-frequency content in the power spectral density (PSD) of data generated by McFarlane's method.[6]

We demonstrate that this hybrid method creates wind time series that closely match the high-frequency and low-frequency characteristics of measured wind data and that the results of wind turbine simulations run with our hybrid wind closely match the results of turbine simulations run with measured wind data.

2. HYBRID METHOD FOR GENERATING WIND DATA

We propose a hybrid method to generate long periods (days to years) of wind speed time-series data by combining measured wind speed statistics sampled at low rates with simulated wind turbulence sampled at high rates. Measured statistics capture the non-stationary properties of real wind, and simulated turbulence interpolates between the measured data. The hybrid method simulates short periods of turbulence using measured mean wind speed (and variance, if available) as a parameter, then superimposes the simulated turbulence on measured mean wind speed.

We define T as the total length of the period covered by the input data (in seconds); the total length of the output data is also T because the hybrid method interpolates the measured data. The sampling interval of the low-rate measured statistics is $T_{\text{sample,input}}$ $(f_{\text{sample,input}})^{-1}$ (we use $T_{\text{sample,input}}$ 600 s, $f_{\text{sample,input}}$ 1.7×10^{-3} Hz). The sampling frequency of the output data is f_{output} (we use $f_{\text{output}} = 1$ Hz).

A hybrid wind speed time series $u(t)$ of length T with output sampling frequency f_{output} is created by the following steps, as illustrated in Figure 1:

A. Statistics of wind speed data are calculated over long intervals. In this paper, the wind speed mean and variance are measured with a sampling interval of $T_{\text{sample,input}} = 600$ s.
B. A block of zero-mean, high-frequency turbulence is simulated for every *two* points of measured data ($2T_{\text{sample,input}}$) using a spectral model and the Veers method.[5] Blocks of turbulence are concatenated together without blending, overlapping or windowing.
C. The measured mean wind speed is re-sampled to the desired sampling rate f_{output} and smoothed by a low-pass filter.
D. The simulated turbulence is added to the smoothed mean to create the hybrid wind speed time series.

Wind Energ. 2012; **15**:699–715 © 2011 John Wiley & Sons, Ltd.
DOI: 10.1002/we

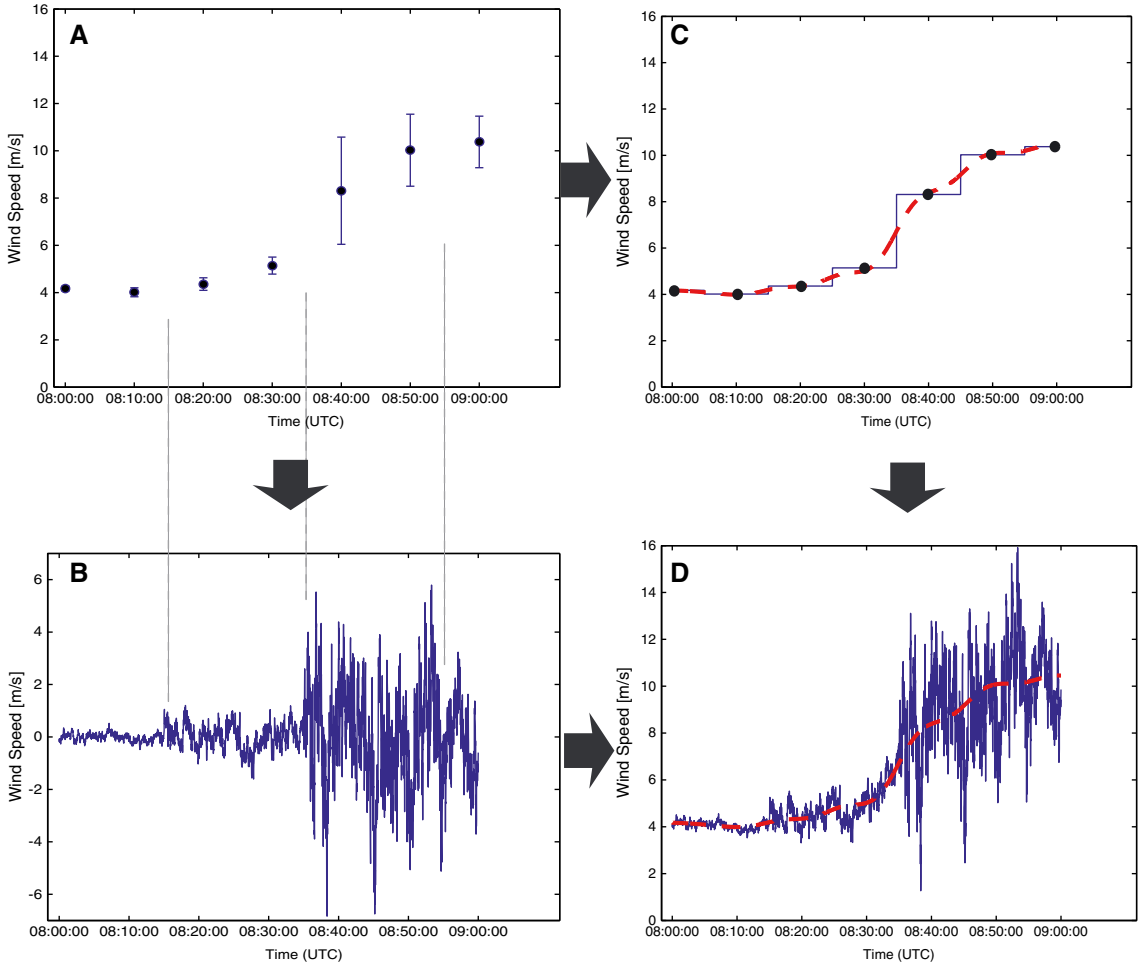

Figure 1. Procedure for generating wind speed time series from a hybrid of measured and simulated data. (a) Wind speed mean and variance measured for a long period $T_{sample,input}$ are used as parameters to generate zero-mean turbulence in (b). The mean wind speeds in (a) are re-sampled at a higher rate f_{output} and smoothed by a low-pass filter in (c). The hybrid wind speed time series in (d) is the sum of (b) and (c).

2.1. Slowly varying measured wind speed (C)

The basis of a hybrid wind time series is mean wind speed measured at sampling intervals of $T_{\text{sample,input}}$. Low-rate mean wind speed captures slow changes such as diurnal and seasonal phenomena and the passing of weather fronts. Meteorological stations for wind resource assessment or weather prediction record the mean (and sometimes variance) of wind speed for periods of a few minutes. In this research, we use measured 10 min mean $U_{0,p}$ and variance $\sigma^2{}_{u,p}$, where p is an index of the 10 min period (Figure 1(a)).

We wish to create a time series of wind speeds of length T with a sampling rate of f_{output}. We re-sample the low-rate mean data to a sampling rate of f_{output} by repeating each measured mean $U_{0,p}$ at intervals f_{output} for a period of $T_{\text{sample,input}}$ (Figure 1(c)). Increasing the sampling rate from $f_{\text{sample,input}}$ to f_{output} does not add any new information, but it adds high-frequency noise.

According to the sampling theorem, the maximum frequency signal that can be resolved by data sampled at $f_{\text{sample,input}}$ is $f_{\text{Nyq,input}} = (2T_{\text{sample,input}})^{-1}$ (the Nyquist frequency);[11] all the content for frequencies higher than $f_{\text{Nyq,input}}$ is introduced as noise. We remove the noise using a third-order low-pass Butterworth filter with a cutoff frequency of $f_{\text{cutoff}} = f_{\text{Nyq,input}} = (2T_{\text{sample,input}})^{-1}$, where the gain of the filter is 1. The low-pass filter is implemented in the frequency domain by applying the Fourier transform to the data, convolving the transformed data with the filter and then applying the inverse Fourier transform. To avoid wrap-around effects from the Fourier transform, we de-trend the data by

subtracting the best-fit line before applying the Fourier transform and then adding that best-fit line after applying the inverse Fourier transform.

2.2. High-rate turbulence (B)

The hybrid method simulates high-rate turbulence to interpolate between measured mean wind speed values, shown in Figure 1(b). For every two measured mean wind speeds $U_{0,p}$ and $U_{0,p+1}$, we generate a zero-mean turbulence time series of length $2T_{\text{sample,input}}$. To model the non-stationary properties of real wind, the variance of each simulated turbulence time series is a function of the corresponding measured mean wind speed (and variance, if available). We model wind turbulence with two variations of the Kaimal spectrum: the form given in Kaimal's original paper that models variance as a function of surface roughness length z_0[12], and the form given in the IEC 61400-1 standard that takes wind speed variance as an explicit input.[13]

Wind turbulence is simulated by a method developed by Shinozuka[14] and extended by Veers.[5] The Veers method simulates wind turbulence by taking the Fourier transform of a turbulence spectrum. The procedure for simulating wind turbulence by Veers method is described in detail in many other sources[5,15] and summarized here:

1. Define a one-sided spectrum for the wind turbulence $S(f)$.
2. Discretize the spectrum for the desired output period and sample rate: $S[m] = S(f)f_{\text{output}}$.
3. Scale the discretized spectrum and apply random phase angles:

$$\mathbf{V}[m] = \sqrt{(1/2)\eta S[m]}e^{i\phi[m]}$$

4. Construct a two-sided spectrum $\mathbf{V}_{2\text{side}}$.
5. Calculate the turbulence time series: $\mathbf{u} = |\text{FFT}(V_{2\text{side}})|$.

If the wind speed variance $\sigma^2{}_u$ is known, the one-sided Kaimal spectral model specified in the IEC 61400-1 standard[13] can be used:

$$S(f) = \sigma_u^2 \frac{4\left(\frac{L_i}{U_0}\right)}{\left(1 + 6\frac{L_i}{U_0}f\right)^{5/3}} \tag{1}$$

If the wind speed variance is not known but the surface roughness length z_0 is known (or can be estimated), the one-sided Kaimal spectral model proposed by Kaimal[12] can be used:

$$S(f) = u_*^2 \frac{105\left(\frac{z}{U_0}\right)}{\left(1 + 33\frac{z}{U_0}f\right)^{5/3}} \tag{2}$$

where $\sigma_u = 10$ min standard deviation of longitudinal wind speed (m s^{-1}),$U_0 = 10$ min mean of longitudinal wind speed (m s^{-1}), $u_*{=}\kappa\ U_0[\ln(z/z_0)]$, $\kappa = 0.4 =$ von Kármán constant, $z =$ turbine hub height (m), $z_0 =$ surface roughness length (m), $f =$ frequency (Hz), $L_1 = 8.1 \times \Lambda_1$ and

$$\Lambda_1 = \begin{cases} 0.7z & z \leq 60m \\ 42 & z > 60m \end{cases}$$

The duration of each simulated interval of high-rate turbulence must be $2T_{\text{sample,input}}$ in order to generate frequency content up to $f_{\text{Nyq,input}}$, the highest frequency that the input data can resolve according to the sampling theorem.[11] Each simulated period will contain $N = 2T_{\text{sample,input}}\ f_{\text{output}}$ points; if N is not an integer, we round it up to the nearest even integer.

Each simulated time series corresponds to two low-rate measurements, so we must combine the measured means $U_{0,p}$ and $U_{0,p+1}$ and the measured variances $\sigma^2{}_{u,p}$ and $\sigma^2{}_{u,p+1}$ according to the following formulas:

$$U_{0,\ p\cup p+1} = \frac{U_{0,p} + U_{0,p+1}}{2} \tag{3}$$

Wind Energ. 2012; **15**:699–715 © 2011 John Wiley & Sons, Ltd.
DOI: 10.1002/we

$$\sigma^2_{u,p\cup p+1} = \frac{\left(\frac{N}{2}-1\right)\sigma^2_{u,p} + \left(\frac{N}{2}-1\right)\sigma^2_{u,p+1}}{N-2} \tag{4}$$

where equation (4) is the formula for the pooled variance of two equally sized samples of $N/2$ points each.[16]

We discretize the continuous one-sided Kaimal spectrum $S(f)$ in equation (1) or (2) at discrete frequencies $f_m = m\Delta f$:

$$\mathbf{S}[m] = S(f_m)\Delta f \quad m = \{0, 1, \ldots, M-1\} \tag{5}$$

There are $M = 1 + N/2$ unique frequencies in the one-sided spectrum, where $N = 2T_{\text{sample,input}}\ f_{\text{output}}$. We require that N be an even integer, so M will be an odd integer based on the definition, We force $S[0] = 0$ because the steady state ('DC') value of the simulated data is zero, and we are simulating a zero-mean process.

We scale the magnitude of the discretized spectrum according to the following formula to create $\mathbf{V}$, a vector of fourier coefficient for a one-sided spectrum:

$$\mathbf{V}[m] = \sqrt{(1/2)\eta\mathbf{S}[m]}e^{i\phi[m]} \tag{6}$$

The term $e^{i\phi[m]}$ creates random phases in $\mathbf{V}$ that make the output of Veers method random. The phases $e^{i\phi[m]}$ are complex numbers, and $S[m]$ are real numbers, so $\mathbf{V}[m]$ are complex numbers. The phase angles $\phi[m]$ are drawn from a uniform random distribution over the range $[0\ 2\pi]$. Nearly all simulations that use the Shinozuka/Veers method use uniform randomly distributed phase angles. Shinozuka proves that a simulated time series will be ergodic if uniform randomly distributed phase angles are used.[15] In our analysis of measured wind speed data sampled at 5–52 Hz, we found that the differences between adjacent phase angles can be described by a von Mises distribution[17] and that the fit of the von Mises distribution improves for higher sampling frequencies. However, we find that it is statistically impossible to distinguish between uniform and von Mises distributions for the sampling frequencies used in our paper ($\sim$1 Hz). The dispersion of the von Mises distribution of the phase differences, analogous to the standard deviation in a normal distribution, is so low at this sampling frequency that statistical tests cannot establish that a von Mises distribution fits the data.

The factor of 1/2 in equation (6) is necessary because we will create a two-sided spectrum from $\mathbf{V}$, but the spectra in equations (1) and (2) are one-sided spectra. The factor of 1/2 should be omitted if a two-sided spectrum is used. We introduce η to normalize $S[m]$ to compensate for the variance lost when $S(f)$ is discretized.

The factor η accounts for the difference between the desired variance ${\sigma^2}_{\text{desired}}$ and the actual variance ${\sigma^2}_{\text{actual}}$ of data simulated with the discretized spectrum in equation (5). We define η as follows:

$$\eta = \frac{\sigma^2_{\text{desired}}}{\int_{\Delta f-\frac{1}{2}\Delta f}^{\Delta f+\frac{1}{2}\Delta f} S(f)df} \tag{7}$$

In theory, the variance σ^2 of wind turbulence simulated from a one-sided spectrum is given by equation (8) and approximated by equation (9); assuming that M is large:

$$\sigma^2 = \int_0^\infty S(f)\mathrm{d}f \tag{8}$$

$$\approx \sum_{m=0}^{M} \mathbf{S}[m] \tag{9}$$

In practice, the actual variance of the simulated wind turbulence is smaller than that predicted in equations (8) and (9) because $S[0] = 0$ and M is not infinite. This is a problem because variance is a parameter in the spectrum in equation (1) and we want the variance of the simulated turbulence output to equal that parameter.

We show in Figure 2 that the actual variance of the simulated turbulence output is well predicted by the following formula:

$$\sigma^2_{\text{actual}} \approx \sum_{m=1}^{M} \mathbf{S}[m] \approx \int_{\Delta f+\frac{1}{2}\Delta f}^{f_{\text{Nyq}}+\frac{1}{2}\Delta f} S(f)\mathrm{d}f \tag{10}$$

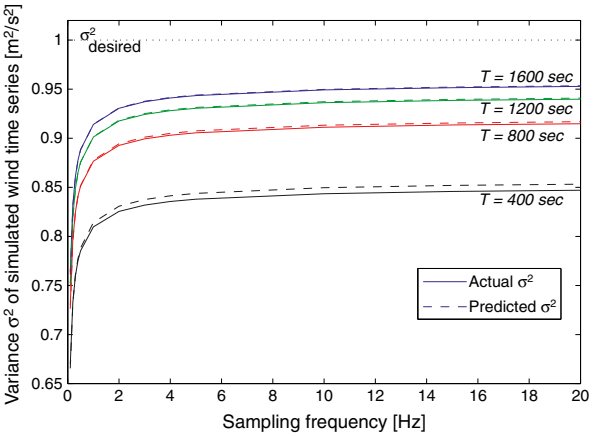

Figure 2. This figure plots the actual variance of turbulence simulated with the Kaimal spectrum in equation (1) and a variance parameter $\sigma^2{}_{\text{desired}} = 1$ against the sampling frequency of the simulation. Different curves plot simulations of different lengths. The actual variance is plotted as solid lines, and the variance predicted by equation (10) is plotted as dotted lines. The turbulence is simulated with Veers method, the Kaimal spectrum from equation (1); $U = 10$ m s^{-1}, $\sigma^2 = 1$ m^2 s^{-2} and z = 65.

where the integration limits in equation (10) are determined by the method for discretizing the continuous spectrum, best illustrated by Figure 1 in a paper by Yang.[18] The integral of the continuous spectrum in a small region around f_m is approximated by a rectangle of height $S[m]$ and width Δf:

$$\mathbf{S}[m]\Delta f \approx \int_{f_m-\frac{1}{2}\Delta f}^{f_m+\frac{1}{2}\Delta f} S(f)\mathrm{d}f \tag{11}$$

Figure 2 shows that discretizing the turbulence spectrum causes a loss of variance in the simulated turbulence. We simulated 400–1600 s of turbulence at sampling frequencies from 0.2–20 Hz using Veers method and the Kaimal spectrum in equation (1). The actual variance of simulated turbulence deviates significantly from the desired variance ($\sigma^2{}_{\text{desired}} = 1$); the actual variance only approaches the desired variance asymptotically with increasing sampling frequency ($f_{\text{output}} \to \infty$) and increasing sample period ($T \to \infty$). In this paper, we use a sampling frequency of 5 Hz and a sampling period of 1200 s, which means that the variance of each period of simulated turbulence is approximately 8% lower than the measured variance used as a parameter in the simulation.

We correct for that loss of variance using equation (10). This equation, plotted as dotted lines, closely predicts the actual variance of simulated turbulence, plotted as solid lines, without running a simulation. We use that prediction to calculate η in equation (7) and use η in equation (6) to scale the spectrum so the variance of the simulated turbulence measured the desired variance.

We use the following pattern to create a two-sided spectrum of N points:

$$V_{2\text{side}} = [0, \mathbf{V}[2], \mathbf{V}[3], \ldots, \mathbf{V}[M-1], |\mathbf{V}[m]|, \mathbf{V}^*[M-1], \ldots, \mathbf{V}^*[2]] \tag{12}$$

where the negative frequencies are represented in the second half of $\mathbf{V}_{2\text{side}}$, each $\mathbf{V}_{2\text{side}}[n]$ is complex valued except $\mathbf{V}_{2\text{side}}[N/2]$, and the first element $\mathbf{V}_{2\text{side}}[1]$ is forced to zero because we are creating a zero-mean simulation. To produce a time series of real-valued wind speeds, the $\mathbf{V}_{2\text{side}}$ must be conjugate symmetric; that is $\mathbf{V}_{2\text{side}}[n] = \mathbf{V}^*_{2\text{side}}[\,\text{mod}\,(N-n+1,\quad N)+1]$, where the * operator represents complex conjugation. Note that the magnitudes of the one-sided spectra in equation (1) or (2) are multiplied by 1/2 in equation (6) in anticipation of creating the two-sided spectrum in equation (12).

We calculate the turbulence time series output $\mathbf{u}$ using the fast Fourier transform (FFT):

$$\mathbf{u} = |\text{FFT}(\mathbf{V}_{2\text{side}})| \tag{13}$$

where the FFT is defined following Press[11] as follows:

$$\mathbf{u}[n] = \sum_{k=1}^{N} \mathbf{V}_{2\text{side}}[k] \mathrm{e}^{i\,2\pi(n-1)(k-1)/N} \quad n = 1, \ldots, N \tag{14}$$

Wind Energ. 2012; **15**:699–715 © 2011 John Wiley & Sons, Ltd.
DOI: 10.1002/we

In theory, it is not necessary to take the absolute value of the FFT in equation (13) because the conjugate-symmetric two-sided spectrum we constructed in equation (12) ensures that the output of the FFT will be real valued. In practice, the limited numerical precision of computers may cause the output $\mathbf{u}[n]$ to have small imaginary values.

Confusingly, different sources define the FFT and its inverse in opposite ways. Press[11] gives the definition of the FFT in equation (14), but Bracewell[19] and Newland[20] define that as the inverse FFT. The MATLAB software (MathWorks, Natick, MA, USA) uses the definition in equation (14) except for a minus sign in the exponential term; Mathematica accepts a parameter for the choice of definitions.

2.3. Combining empirical and simulated data (D)

We create the hybrid wind speed time series by concatenating the blocks of simulated zero-mean turbulence and superimposing them on the filtered measured mean data (Figure 1(d)). We find that windowing the periods of simulated turbulence suggested by some authors[6,9] is not necessary. We do not encounter the problem of excessive spectral content at low frequencies noted by McFarlane[6] because our method does not overlap consecutive blocks of simulated high-frequency data and because we low-pass filter the measured data.

2.4. Extension to three dimensions

We do not consider the general three-dimensional case of the Veers method here; good explanations can be found in the papers of Veers[5] and Sørensen,[4] but we will briefly summarize how to extend the one-dimensional case described earlier. A simulated three-dimensional wind field consists of parallel, coherent one-dimensional wind speed time series. A coherence matrix γ is introduced in equation (6), so the discretized spectrum $\mathbf{S}[m]$ must be a square matrix. Because $\mathbf{S}[m]$ is a square matrix, the square root operation must be replaced by the Cholesky decomposition or similar decomposition that yields a lower-triangular matrix. Similarly, the random phases in the $e^{i\phi[m]}$ term of equation (6) must be replaced by a square matrix with complex random phase angles on the diagonal and zeros elsewhere.

2.5. Application notes

The general method we present here can be used to generate high-frequency wind speed time-series data. However, certain applications require details we have not discussed earlier.

2.5.1. Power production.

The large rotors on multimegawatt wind turbines filter most high-frequency turbulence but make the power output of those turbines sensitive to the significant wind speed differences across the rotor induced by shear. Wagner has shown that calculating the power performance of a wind turbine from only hub-height wind speed measurements introduces significant uncertainties;[21] related research by Antoniou has shown hub-height measurements introduce similar uncertainties in power curve and wind resource calculation.[22] Wagner proposes several methods to calculate an 'equivalent' wind speed that better correlates with power output.[21] Dolan proposes an alternative formula to calculate an equivalent wind speed based on a wind shear function.[23] These methods calculate an equivalent wind speed from wind speeds measured at several heights within the area of the turbine rotor. Our hybrid method can be used to generate wind speed times series at multiple heights, but the results will be sensitive to the models of wind shear and vertical coherence used. We also recommend simulating the low-pass filtering effect of the large rotor with the $H_{\psi,0}(s)$ filter proposed by Sørensen.[24].

2.5.2. Power quality/flicker.

Power quality and flicker analyses deal with power variations at frequencies higher than approximately 1 Hz.[25] The large rotor of multimegawatt wind turbines filters most wind fluctuations at frequencies higher than 10^{-1} Hz,[26] but wind shear and the aerodynamic effect of blades passing the tower introduce noise at three times the rotation frequency ("3p"). We recommend applying the $H_{\psi,0}(s)$ and $H_{\psi,3}(s)$ filters proposed by Sørensen[24] to simulate the low-pass filtering effect of the large rotor and the 3p effect of wind shear and blades passing the tower.

3. VALIDATION

We validate the method for creating hybrid wind speed data described previously by comparing the data it generates with the wind speed data measured at three sites in the USA The hybrid method was created to support simulations of wind power variability on time scales relevant to grid frequency regulation, so we focus on validating the characteristics of the hybrid method that are most important for that application. First, we compare the characteristics of wind speed variation,

especially the PSD. Then we use that wind speed data to drive a simulated wind turbine to create wind power data. We compare the energy production and ramp rate characteristics of the wind power over different time scales.

The procedure for creating the data used to validate the hybrid wind method is as follows:

1. Collect measured wind speed data from field measurements (see Table I) and decimate data to 5 Hz. The measured 5 Hz data are the 'Measured' data set.
2. Calculate 10 min statistics (mean and standard deviation) from measured wind data in step 1. The measured 10 min mean wind speeds (resampled to 5 Hz) are the 'Measured, 10-min avg' data set.
3. Generate 5 Hz hybrid wind speed data.
   a. Hybrid data created with equation (1), which takes wind speed standard deviation as an input, are the 'Hybrid, σ' data set.
   b. Hybrid data created with equation (2), which takes estimated surface roughness length as an input, are the 'Hybrid, z_0' data set.
4. Simulate time series of the power output of a 2 MW wind turbine, using the wind speed time series generated in Step 3.

3.1. Validation data

To validate our hybrid method of creating long wind speed time series, we used publically available wind speed data from three experiments conducted by the U.S. National Center for Atmospheric Research: Cooperative Atmosphere-Surface Exchange Study (CASES99),[27] Fluxes over Snow Surfaces, Phase II (FLOSSII)[28] and Advanced Technology Solar Telescope (ATST) site survey,[29,30] summarized in Table I. We decimate these data to 5 Hz by applying an eighth-order low-pass Chebyshev Type I filter and then down-sampling the data by selecting every rth point, where r is the sampling frequency of the data set divided by 5 Hz.[31] We calculate the along-wind horizontal (longitudinal) wind speed from the decimated data. The large rotor on modern wind turbines acts as a low-pass filter to attenuate phenomena faster than approximately 0.5 Hz,[26] so we choose a sampling rate of 5 Hz to ensure we capture all significant power variations.

We group the data into contiguous blocks that share common atmospheric stability properties. First, we calculate the stability criterion value $1/L$ for each 1 h period, where L is the Obukhov length from Businger[32] calculated according to equation (15). Next, we determine the Pasquill atmospheric stability class[33] corresponding to the calculated value of $1/L$ using a nomogram given by Golder,[34] assuming the roughness lengths z_0 given in Table I. Finally, we create each block of data by selecting the contiguous data with the same stability class: stable (Pasquill A, B, C), neutral (Pasquill D) or unstable (Pasquill E, F) and require that each block of data be a minimum of 2 h long and have a mean wind speed greater than 4 m s^{-1}. The distribution of the data in the stability classes is shown in Table II.

$$L = \frac{u_*^3 \overline{T}}{\kappa g \overline{w' T_v'}} \tag{15}$$

Table I. Properties of data sets from three U.S. National Center for Atmospheric Research experiments used to validate the hybrid wind model.

Data set name name	Location	Measurement height [m]	Sampling frequency [Hz]	Surface roughness z_0 (estimated) [m]	Dates sampled
CASE99	Leon, Kansas	55	20	0.03	6–30 October 1999
FLOSSII	North Park, Colorado	30	60	0.03	20–31 November 2002 15–29 December 2002
ATST	Big Bear Lake, California	25	30	0.003	7 May – 14 June 2004

CASES99, Cooperative Atmosphere-Surface Exchange Study; FLOSSII, Fluxes Over Snow Surfaces, Phase II; ATST, Advanced Technology Solar Telescope.

Table II. Distribution of the measured wind speed data in different atmospheric stability classes.

Data set	Stable data [hours]	Neutral data [hours]	Unstable data [hours]
CASES99	148	177	10
FLOSII	111	150	0
ATST	46	87	111

CASES99, Cooperative Atmosphere-Surface Exchange Study; FLOSSII, Fluxes over Snow Surfaces, Phase II; ATST, Advanced Technology Solar Telescope.

Wind Energ. 2012; **15**:699–715 © 2011 John Wiley & Sons, Ltd.
DOI: 10.1002/we

where $u_* = \left(\overline{u'w'}^2 + \overline{v'w'}^2\right)^{1/4}$ = friction velocity (definition from Weber[35]), u = longitudinal (along-wind) velocity (m s^{-1}),v = latitudinal (across-wind) velocity (m s^{-1}), w = vertical wind velocity (m s^{-1}),T = absolute temperature (K),T_v = virtual temperature ($^\circ C$), $\kappa = 0.4$ = von Kármán constant,$g = 9.8$ m s^{-2} = acceleration of gravity and $\overline{a'b'}$ = covariance of two variables a and b.

3.2. Wind speed time series

Figure 3 qualitatively compares wind speed time series generated with our hybrid method to a measured wind speed time series. The two hybrid wind speed data sets ("Hybrid, σ" and "Hybrid, z_0") are generated by calculating the 10 min mean and variance of the measured time series, then superimposing simulated high-frequency turbulence on the 10 min mean data. For comparison, the 'Measured, 10-min avg' plot shows the kind of measured data commonly captured from meteorological masts that would be used as the basis for generating hybrid wind data.

The plots in Figure 3 demonstrate that the hybrid method generates realistic non-stationary wind speed data. We calculate the 10 min means and variances of a 5 h period of empirical wind speed data, labeled 'Measured', that has a significant increase in mean wind speed beginning at $t = 3000$ s and a significant increase in wind speed variance beginning at $t = 7000$ s. Wind speed with the data simulated with the 'Hybrid, σ' method, which takes mean and variance as inputs, captures the increase in mean wind speed and the increase in variance. Wind speed with the data simulated with the 'Hybrid, z_0' method, which takes only the mean as an input, also captures the increase in mean wind speed and the increase in variance.

3.3. Wind turbulence spectra

We compare the PSD of hybrid wind speed time series with the PSD of measured wind speed time series from the CASES99 experiment. We calculate the PSD according to the following formula:

$$S_{2\text{side}}(f) = T\,|\text{FFT}^{-1}(\mathbf{u})|^2 \tag{16}$$

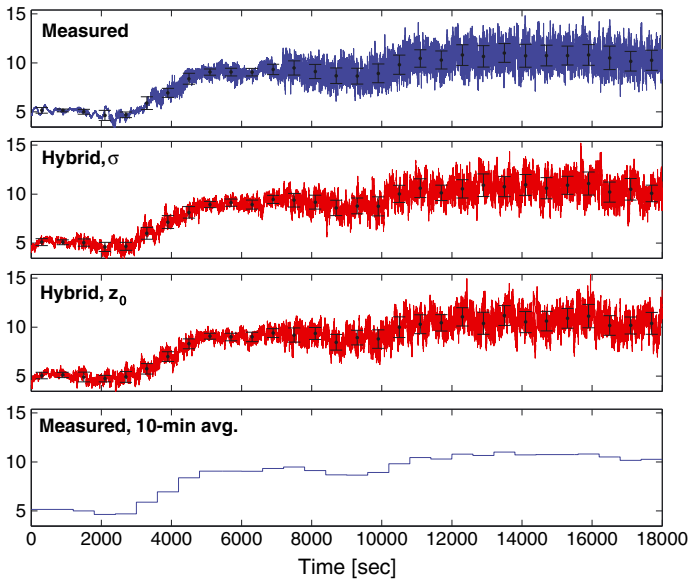

Figure 3. A comparison of measured wind speed data ('Measured'), hybrid wind speed data generated with empirical mean and variance statistics ('Hybrid, σ'), hybrid wind speed data generated with empirical mean statistics and estimated surface roughness length ('Hybrid, z0'), and empirical mean statistics ('Measured, 10-min avg'). These data are representative of the close match between hybrid wind speed data and measured data with similar statistical properties. These plots show 5 h of data from the CASES99 experiment beginning at 8 PM on 28 October 1999 (stable atmospheric conditions). The hybrid and 'Measured, 10-min avg' data are generated using 10 min statistics derived from the 'Measured' data.

where T is the duration of the data in second and the inverse Fourier transform is defined by Press[11] as follows:

$$\mathbf{V}_{2\text{side}}[k] = \frac{1}{N}\sum_{n=1}^{N}\mathbf{u}[n]e^{-i2\pi(n-1)(k-1)/N} \quad k = \{1,\ldots,N\} \tag{17}$$

Each PSD plotted in Figure 4 is the average of all the PSDs of 2 h periods with the mean wind speed between 6 and 8 m s^{-1}. This averaging, called 'segment averaging' in Press, Section 13.4[11] reduces the variance of the PSD. The number of periods averaged is given in the title of each plot. We plot the spectra for mean wind speeds 6–8 m s^{-1} because that range consistently contains the most data across the three experimental sites. We plot the spectra of four different data sets: 'Measured' is ATST field data decimated to 5 Hz, 'Hybrid, σ' is hybrid data created with the Kaimal spectral model in equation (1), 'Hybrid, z_0' is hybrid data created with the Kaimal spectral model in equation (2) and 'Measured, 10-min avg' is 10 min means of the ATST field data, re-sampled to 5 Hz by repeating each value. We include the 'Measured, 10-min avg' data to show the results if 10 min average data are re-sampled to a higher frequency without adding high-frequency turbulence. The spectrum of the 'Measured, 10-min avg' data diverges from the spectrum of the 'Measured' data for two reasons. First, calculating the 10 min average of the 'Measured' data acts as a low-pass filter that attenuates the spectral power beginning at approximately 10^{-3} Hz. Second, re-sampling 10 min average data to create the 'Measured, 10-min avg' data introduces noise at frequencies f 1.7×10^{-3} Hz with spectral power that decreases as f^{-2}.

Figure 4 demonstrates the advantage of the hybrid method: it adds the turbulence not found in the 10 min average data (plotted in green). The spectra of the hybrid wind data in Figure 4 closely match the spectra of the measured ATST wind data in stable, neutral and unstable atmospheric conditions. The spectra of wind speed data generated with both hybrid variants are almost indistinguishable from the spectra of the measured data at all frequencies. These results are representative of the results for other range of mean wind speed and for data from the CASES99 and FLOSSII experiments with one exception: the hybrid wind under-predicts the magnitude of turbulence for frequencies in the range of 1×10^{-3} – 3×10^{-3} Hz when compared with data from the CASES99 test site during stable atmospheric conditions (not shown). That range of frequencies is where measured data are joined with simulated turbulence to form hybrid wind, which suggests that the low-pass filter applied in step C of the hybrid method may not be steep enough. However, this under-prediction is not evident in neutral and unstable CASES99 data or in any of the ATST and FLOSSII data.

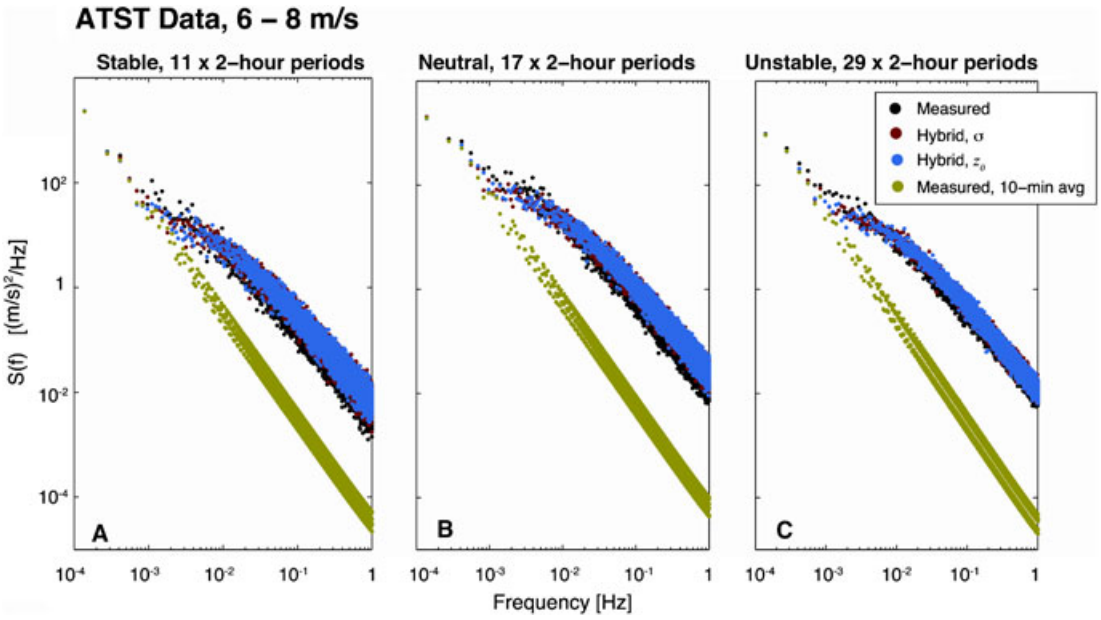

Figure 4. A comparison of power spectral densities (PSD) of measured wind data, both variants of hybrid wind speed data, and measured 10 min average data from the ATST field site for 6–8 m s^{-1} mean wind speed. Each PSD is the segment average of the PSDs all 2 h segments of data in the specified mean wind speed range (see description in text). Data from stable conditions ($0.01 < 1/L < 0.15$) are plotted in (a), neutral conditions ($-0.03 < 1/L < 0.01$) are plotted in (b) and unstable conditions (-0.15 $1/L < -0.03$) in (c). We plot the spectral only to 2 Hz because we decimate (low-pass filter and down-sample) the measured data to 5 Hz, but the low-pass filtering attenuates the spectra of the measured data above 2 Hz.

Wind Energ. 2012; **15**:699–715 © 2011 John Wiley & Sons, Ltd.
DOI: 10.1002/we

3.4. Wind turbine simulation model

All wind power data used in this paper are created by simulation of a single 2 MW wind turbine in MATLAB/Simulink. The turbine is a pitch-regulated, variable-speed model with an 80 m rotor, modeled using the Wind Turbine Blockset, v3.0 developed by Aalborg University.[36] This simulation model is not a static power curve; it models the dynamics of rotor acceleration and pitch and torque regulation. It does not model electrical transients or the 3p blade-passing frequency. We use the turbine design parameters, control scheme, control parameters and first-order generator model recommended by the Danish Technical University.[37] We incorporate a rotor-wind filter $H_{\psi,0}(s)$ proposed by Sørensen[24] into the wind turbine model to simulate the filtering effect of a large rotor on turbulence that is not spatially homogeneous, but we do not account for the effect of vertical wind shear across the rotor disk.

Each simulation takes wind speed sampled at 5 Hz as its input and generates real power sampled at 5 Hz as its output. We initialize each simulation by duplicating the initial wind speed value for 1000 s at the beginning of wind speed data set; this padding allows initial transients of the simulation model to settle out. We remove the corresponding first 1000 s of the output power data. As described in Section 3.1, each input data set consists of at least two contiguous hours of wind speed data in one stability regime (stable, neutral, or unstable) with a mean wind speed greater than 4 m s^{-1}.

3.5. Validation of power production

We compare the energy and power produced by one 2 MW wind turbine with 40 m blades (described in Section 3.4) fed with both the measured and hybrid wind speed time series. Comparing simulated wind power takes into account the filtering effect of a large wind turbine on wind speed fluctuations and the dynamic response of a modern turbine to those fluctuations. We do not compare simulated wind power to wind power measured from actual wind turbines because of the difficulties in controlling the output of actual turbines for wind direction, wakes, terrain, mechanical and electrical losses, power limits and ramp rate limits. Future work should analyse met-mast and wind power data to give a more thorough comparison of the hybrid method to the output of an actual wind turbine.

Figure 5 shows a comparison between the energy generated by a 2 MW wind turbine driven by the measured wind data described in Table I and the corresponding hybrid wind data. Each subplot shows the percent error in energy generation in 1 h periods plotted against the mean power for that 1 h period, measured in the *per-unit* (p.u.) system. We use the p.u. system to express turbine power output as a fraction of the maximum power output (2 MW in our paper). Figure 5(a) compares hybrid wind data generated using equation (1), which takes wind speed standard deviation as a parameter. Figure 5(b) compares hybrid wind data generated using equation (2), which takes surface roughness length as a parameter. Figure 5(c) compares measures 10 min average wind data to show the results if the hybrid method is not used to fill in high-frequency turbulence.

We define the 1 h percent energy generation error ε in hour k as follows:

$$\varepsilon(k) = \frac{E_{\text{means}}(k) - \text{E}_{\text{hyb}}(k)}{E_{\text{meas}}(k)} \tag{18}$$

where $E_{meas}(k)$ is the energy generated by the simulated wind turbine driven by measured wind data in hour k and $E_{hyb}(k)$ is the energy generated with hybrid wind data in hour k.

Figure 5 shows that both variants of hybrid wind (Figure 5 (a),(b)) have smaller errors in energy production than the 10 min average data (Figure 5 (c)) they are based on. The mean error for hybrid data created with both methods (A and B) is -0.4%; the mean error for the 10 min average data (C) is -0.8%. Hybrid data also give significantly less variance in the errors: 90% of the hybrid errors falls between -2.7% and +1.4%, whereas 90% of the errors for the 10 min average data falls between -4.5% and 3.4%. Using the hybrid method to add high-frequency turbulence to low-frequency measured data significantly reduces the magnitude and range of error in energy production. The hybrid method also reduces the trend of energy error increasing as a function of mean power: Figure 5 (c) shows that using 10 min average data over-predicts energy production when the average power is low and under-predicts energy when the average power is high. Data created with the hybrid method do not show such a strong trend.

3.5.1. Power ramp rate.

Figures 6 and 7 show comparisons of the ramp rates of power generated by a 2 MW wind turbine driven by the measured wind data described in Table I to the corresponding hybrid wind data. Validation of the ramp rates is important to confirm that the hybrid method accurately models the variations on different time scales. Figure 6 shows a comparison of the distribution of sizes of ramp events, and Figure 7 compares the size of extreme ramp events.

We use the definition that the ramp rate is the change in mean power from one period to the next: $P_{\text{ramp}}(n) = P_{\text{mean}}(n+1) - P_{\text{mean}}(n)$.[38] The ramp rates are binned by the mean power of the starting period $P_{\text{mean}}(n)$. We analyse ramp rates over three different time scales: 10 min, 1 min and 10 s. The 10 min ramp rates correspond to

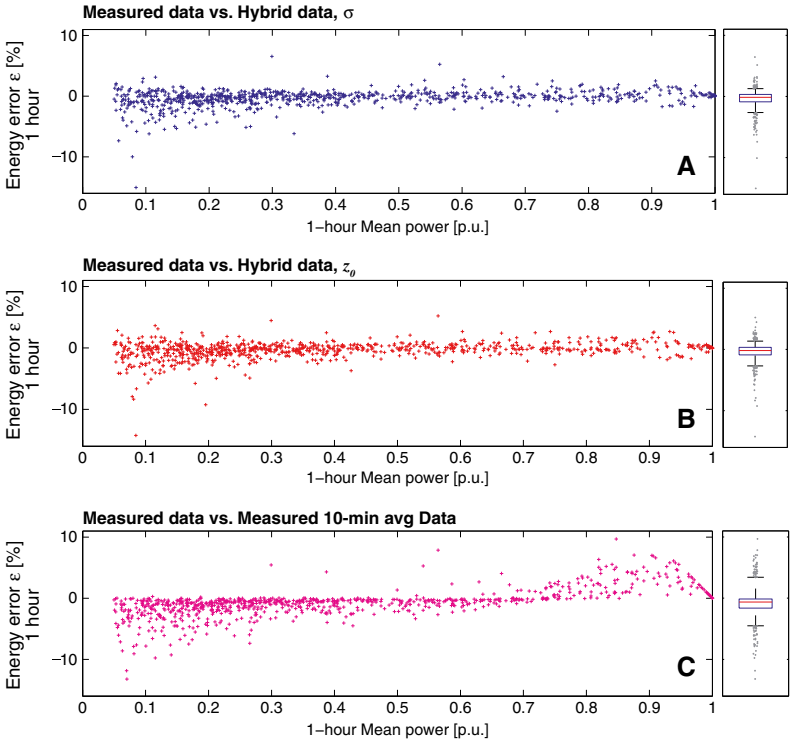

Figure 5. The plots on the left show percent difference in energy production ε between turbine simulated with empirical wind data and that simulated with hybrid wind data, plotted against per-unit (p.u.) mean power. (a) compares measured data to hybrid data created with equation (1), (b) compares measured data to hybrid data created with equation (2), and (c) compares measured data to 10 min average measured data. The boxplots on the right plot the mean (center line), the 25th and 75th percentile values (bottom and top of box) and the 5th and 95th percentiles (bottom and top 'whiskers') of the same data.[40]

phenomena in the 'load-following' time scale, 1 min ramp rates correspond to phenomena in the 'frequency-regulation' time scale, and the 10 s ramp rates correspond to 'flicker' phenomena.

The duration curves in Figure 6 plot the percentile values of ramp rates. Ramp events are grouped together in bins by initial power $P_{\text{mean}}(n)$; Figure 6 shows the duration curves for 10 min, 1 min and 10 s ramp events with an initial power of 0.6 to 0.7 p.u. This figure is similar to comparisons of measured and simulated wind power ramp rates given by Brower for validation of the Eastern Wind Integration and Transmission Study, but we plot a cumulative distribution function where Brower plots a probability density function.[39]

Figure 6 shows that the hybrid methods are slightly worse at modeling 10 min ramp rates than 10 min average measured data (A) but much better at modeling 1 min and 10 s ramp rates (B and C). For 10 min ramp rates starting from the 0.6–0.7 p.u. power range (Figure 6(a)), the mean-square error (MSE) between the measured data and the 10 min average measured data is 8.7×10^{-5} p.u./10 min, significantly smaller than MSEs for the two hybrid data sets: 3.3×10^{-4} p.u./10 min and 2.2×10^{-4} p.u./10 min. For 1 min ramp rates (Figure 6(b)), the MSE for the hybrid data sets is 1.9×10^{-4} p.u./1 min, but the MSE for the 10 min average measured data is more than an order of magnitude larger: 5.9×10^{-5} p.u./1 min. For 10 s ramp rates (Figure 6(c)), the MSEs for the hybrid data sets are 3.0×10^{-5} and 6.7×10^{-5} p.u./10 s, but the MSE for the 10 min average measured data is two orders of magnitude larger: 4.9×10^{-3} p.u./10 s. These results are typical of those in all other initial power ranges.

The power ramp rates based on hybrid wind data match very closely to the power ramp rates based on the measured wind over time scales from 10 min to 10 s. The good match between hybrid and measured ramp rates on these time scales shows that the simulated turbulence introduced by the hybrid method models the characteristics of actual wind turbulence well. It is somewhat surprising that the hybrid wind predicts 10 min power ramps that are smaller than 10 min average measured data because the hybrid method adds zero-mean turbulence that should not affect the 10 min ramp rate. We suspect that the under-prediction of 10 min ramp rates by the hybrid method is an artifact of the low-pass filter used in creating the hybrid data. Figure 4 supports this hypothesis—the spectra of hybrid wind diverge slightly from the spectra of measured wind at approximately 1.1×10^{-3} Hz, which corresponds to a period of $\sim$15 min.

Wind Energ. 2012; **15**:699–715 © 2011 John Wiley & Sons, Ltd.
DOI: 10.1002/we

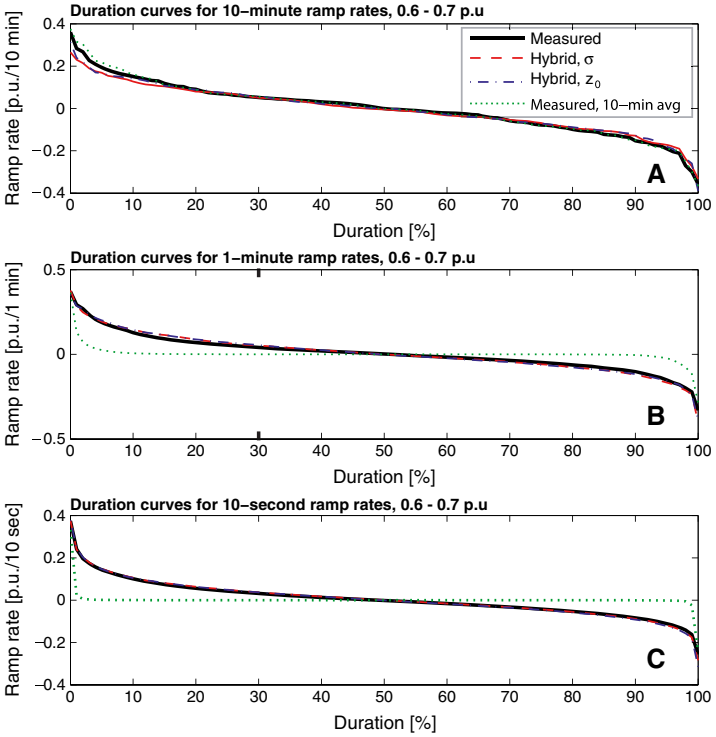

Figure 6. A comparison of the distribution (percentiles) of power ramp rates for a simulated turbine driven by measured wind data. All plots show changes in power starting in the range 0.6–0.7 per-unit (p.u.); (a) shows the distribution of 10 min ramp rates, (b) the distribution of 1 min ramp rates, and (c) the distribution of 10 s ramp rates. The hybrid data are nearly indistinguishable from the measured data, especially for 1 min and 10 s ramp rates.

Figure 7 plots the first percentile (most extreme down ramps) 10 min, 1 min and 10 s ramp rates as a function of initial power $P_{\text{mean}}(n)$. The data are grouped by initial power into 0.1 p.u. bins, so each plotted point is the first percentile ramp rate value for all the data in a particular bin. These plots are a cross-sectional slice of the plots in Figure 6, but varying the initial power instead of the percentile value. The first percentile ramp rates are significant because they put the greatest burden on other generators to compensate for the decrease in wind power.

The data for extreme power ramp rates plotted in Figure 7 show a similar trend to the data in Figure 6: the hybrid data model power ramps over short periods (1 min and 10 s) better than the 10 min average data but slightly worse for 10 min ramping periods. For the first percentile 10 min ramp rates (Figure 7(a)), the MSE between the measured data and the 10 min average measured data is 4.0×10^{-4} p.u./10 min, significantly smaller than the MSEs for the two hybrid data sets: 1.9×10^{-3} p.u./10 min and 1.5×10^{-3} p.u./10 min. For the first percentile 1 min ramp rates (Figure 7(b)), the 10 min average measured data have an MSE of 1.0×10^{-2} p.u./1 min, several orders of magnitude larger than the MSEs of the hybrid data: 8.2×10^{-5} and 6.9×10^{-5} p.u./1 min. Similarly for the first percentile 10 s ramp rates (Figure 7 (c)), the 10 min average measured data have an MSE of 1.4×10^{-2} p.u./10 s, which is two orders of magnitude larger than the MSEs of the hybrid data: 3.1×10^{-4} and 2.4×10^{-4} p.u./10 s.

Similar to the ramp rate duration curves in Figure 6 , the first percentile power ramp rates based on hybrid wind data match very closely to the power ramp rates based on measured wind over time scales from 10 min to 10 s. They do not match as well on a time scale of 10 min—we suspect that the under-prediction of 10 min ramp rates by the hybrid method is an artifact of the low-pass filter used in creating the hybrid data. However, we are surprised that the hybrid data sets diverge significantly at higher initial powers. The hybrid method under-predicts extreme down ramp rates by 2.5% of the rated turbine power output (0.025 p.u.) for initial power 0.8–0.9 p.u., suggesting that the hybrid method generates too much turbulence at higher wind speeds.

3.6. Validation of spinning reserve requirements

Figure 8 compares the power reserves needed for power generated by a 2 MW wind turbine driven by the measured wind data described in Table I and the corresponding hybrid wind data. Validation of the power reserve requirements

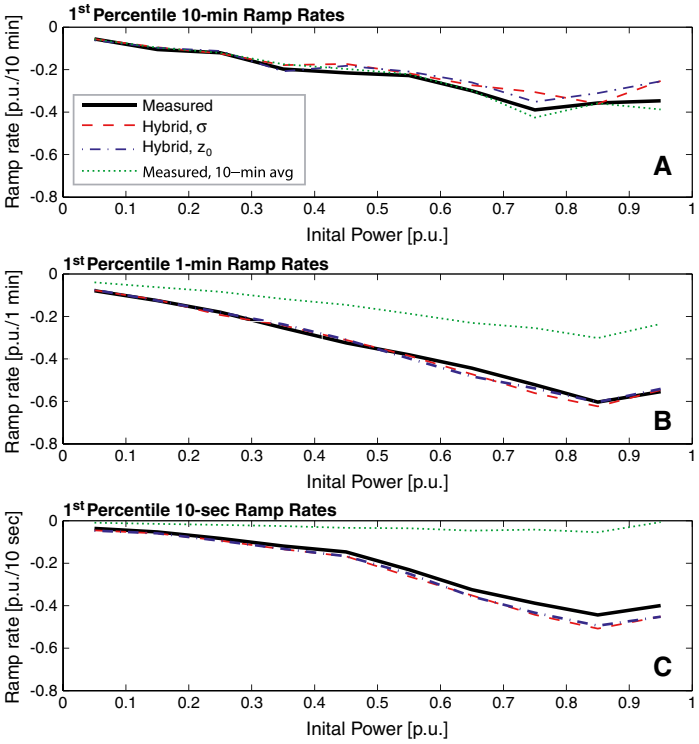

Figure 7. The extreme (first percentile) power ramp rates for a simulated turbine driven by measured and hybrid wind data. Each plot shows the extreme power down ramp as a function of the initial power (power output at the start of ramping). (a) shows the distribution of extreme 10 min ramp rates, (b) the distribution of extreme 1 min ramp rates, and (c) the distribution of extreme 10 s ramp rates. The ramp rates of the hybrid data closely match the ramp rates of the measured data, but the hybrid data predict more extreme 10 s ramp rates for initial power output in the range 0.7 – 1 p.u.

is important to confirm that the hybrid method accurately models the variations on different time scales. We define the reserve requirement as the difference between mean power in one period and minimum power in the next: $P_{\text{ramp}}(n) = P_{\text{mean}}(n) - P_{\text{min}}(n+1)$.[38] The reserve requirement values are binned by the mean power of the starting period $P_{\text{mean}}(n)$. As we did for the ramp rates, we analyse reserve requirements on 10 min, 1 min and 10 s time scales. We analyse the 99th percentile reserve requirements because these represent the most extreme reserve requirements.

The data for extreme power reserve requirements plotted in Figure 8 show that the hybrid method is consistently better at predicting reserve requirements than the 10 min average measured data. For 10 min reserve requirements (Figure 8 (a)), the 10 min average data are nearly as good as the hybrid data: it has an MSE of 4.5×10^{-4} p.u. compared with the MSEs of the hybrid data of 3.8×10^{-4} and 4.5×10^{-4} p.u. For 1 min reserve requirements (Figure 8 (b)), the hybrid method is significantly better: the MSE for 10 min average data is 3.8×10^{-3} p.u., an order of magnitude worse than the MSEs for the hybrid data of 3.0×10^{-4} and 9.7×10^{-5} p.u. For 10 s reserve requirements (Figure 8(c)), the MSE for 10 min average data is 2.6×10^{-3} p.u., and the MSEs for the hybrid data are an order of magnitude smaller: 4.6×10^{-4} and 3.9×10^{-4} p.u.

As with the extreme ramp rates in Figure 7, the hybrid data sets diverge significantly at higher initial powers. The hybrid method over-predicts extreme reserve requirements by 3% of rated turbine power output (0.03 p.u.) for initial power 0.8–0.9 p.u. This result again suggests that the hybrid method generates too much wind turbulence at higher wind speeds.

4. CONCLUSIONS

We demonstrate a method for creating long wind speed time series as a hybrid of measured and simulated wind speed. This method is meant to take advantage of the wind speed data measured at low frequencies by meteorological stations and wind farm developers and the data simulated with appropriate spatial and temporal resolution by mesoscale weather models. The measured wind data capture non-stationary phenomena such as diurnal variations, the passing of weather systems, and

Wind Energ. 2012; **15**:699–715 © 2011 John Wiley & Sons, Ltd.
DOI: 10.1002/we

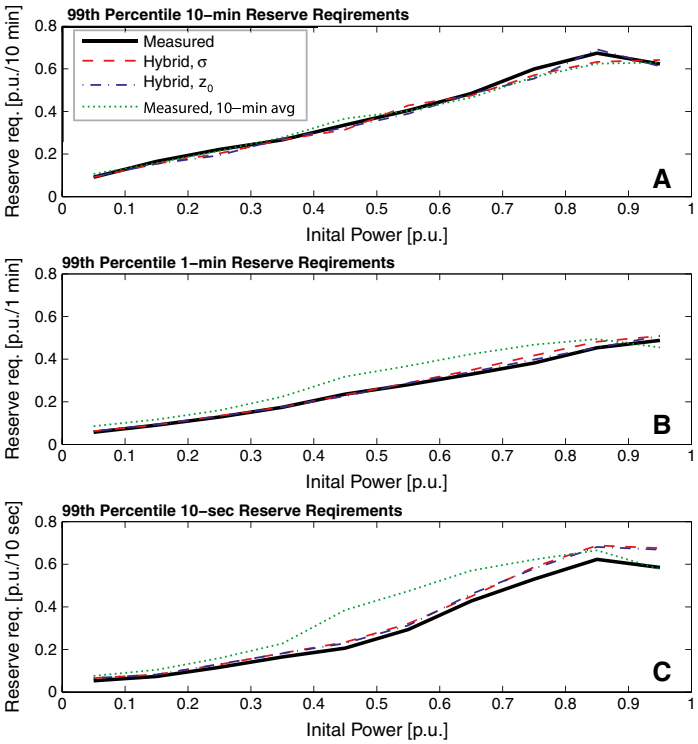

Figure 8. The extreme (99th percentile) reserve requirements for a simulated turbine driven by measured and hybrid wind data. Each plot shows the extreme reserve requirement as a function of the initial power (power output at the start of ramping). (a) shows the distribution of extreme 10 min reserves, (b) the distribution of extreme 1 min reserves, and (c) the distribution of extreme 10 s reserves. The reserve requirements of the hybrid data closely match the reserve requirements of the measured data, but the hybrid data predict more extreme 10 s reserve requirements for initial power output in the range 0.7 – 1 p.u.

seasonal variations, whereas our hybrid method simulates data to interpolate the fast turbulent variations that are needed to accurately model fast variations in wind power.

Our analysis shows that the wind speed time series created with our hybrid method accurately reproduce measured wind speed data from three different sites and in neutral, stable and unstable atmospheres. We demonstrate that the total energy produced by a wind turbine simulated with hybrid wind is within -2.7%/+1.4% of the energy produced by the same turbine simulated with measured wind data for 90% of the tested period. We also demonstrate that the power ramp rates and spinning reserve requirements for a turbine simulated with hybrid wind data very closely match the results for a turbine simulated with measured wind data.

This method is well suited to studies of single wind turbine power fluctuations on the scale of seconds to minutes. It generates wind speed data time series sampled fast enough to simulate dynamic behavior of an individual wind turbine, such as pitch control, but retains their time-dependent characteristics such as diurnal variations, the passing of weather fronts, and seasonal variations.

ACKNOWLEDGEMENTS

The authors thank Mitch Small for his advice on statistical methods. This work was supported in part by a grant from the Alfred P. Sloan Foundation and EPRI to the Carnegie Mellon Electricity Industry Center, the Doris Duke Charitable Foundation, the Department of Energy National Energy Technology Laboratory and the Heinz Endowments for support of the RenewElec program at Carnegie Mellon University. This research was also supported through the Climate and Energy Decision Making (CEDM) center funded under NSF grant SES-0949710 to Carnegie Mellon University.

REFERENCES

1. National Oceanic and Atmospheric Administration. Automated surface observing system (ASOS) user's guide. [cited 2010 Oct 11]; Available from: http://www.nws.noaa.gov/asos/aum-toc.pdf.
2. Kareem A. Numerical simulation of wind effects: a probabilistic perspective. *Journal of Wind Engineering & Industrial Aerodynamics* 2008; **96**(10-11): 1472–1497. DOI: 10.1016/j.jweia.2008.02.048.
3. Nichita C, Luca D, Dakyo B, Ceanga E. Large band simulation of the wind speed for real time wind turbine simulators. *IEEE Transactions on Energy Conversion* 2002; **17**(4): 523–529. DOI: 10.1109/TEC.2002.805216.
4. Sørensen P, Cutululis N, Vigueras-Rodríguez A, Madsen H, Pinson P, Jensen L, et al. Modelling of power fluctuations from large offshore wind farms. *Wind Energy* 2008; **11**(1): 29–43. DOI: 10.1002/we.246.
5. Veers P. Modeling stochastic wind loads on vertical axis wind turbines. *SAND83-1909* 1984; **19**: 1–12.
6. McFarlane A, Veers P, Schluter L. Simulating high-frequency wind for long durations, *13th AMSE Wind Energy Symposium*, New Orleans, LA, 1993.
7. Kelley N, Sutherland H. Damage estimates from long term structural analysis of a wind turbine in a US wind farm environment, *16th ASME Wind Energy Symposium*, Reno, NV, 1997.
8. Negra N, Holmstrøm O, Bak-Jensen B, Sørensen P. Model of a synthetic wind speed time series generator. *Wind Energy* 2010; **11**: 193–209. DOI: 10.1002/we.244.
9. Smallwood D, Paez T. A frequency domain method for the generation of partially coherent normal stationary time domain signals. *Shock and Vibration* 1993; **1**(1): 45–53.
10. Nielsen M, Larsen G, Hansen K. Simulation of inhomogeneous, non-stationary and non-Gaussian turbulent winds. *Journal of Physics: Conference Series* 2007; **75**: 012060. DOI: 10.1088/1742-6596/75/1/012060.
11. Press W, Teukolsky S, Vetterling W, Flannery B. *Numerical Recipes 3 rd Edition: The Art of Scientific Computing*. Cambridge University Press: Cambridge, UK, 2007.
12. Kaimal J, Wyngaard J, Izumi Y, Coté O. Spectral characteristics of surface-layer turbulence. *Quarterly Journal of the Royal Meteorological Society* 1972; **98**: 563–589.
13. International Electroctechnical Commission. *IEC 61400-1: Wind turbines—part 1: design requirements*, 3rd ed. International Electrotechnical Commission: Geneva, 2005.
14. Shinozuka M, Jan C. Digital simulation of random processes and its applications. *Journal of Sound and Vibration* 1972; **25**(1): 111–128. DOI: 10.1016/0022-460X(72)90600-1.
15. Shinozuka M, Deodatis G. Simulation of stochastic processes by spectral representation. *Applied Mechanics Reviews* 1991; **44**(4): 191–203. DOI: 10.1115/1.3119501.
16. Bethea RM, Rhinehart RR. *Applied Engineering Statistics*, 1st ed. CRC Press: Boca Raton, FL, 1991.
17. Fisher N. *Statistical Analysis of Circular Data*. Cambridge University Press: Cambridge, UK, 1993.
18. Yang J. On the normality and accuracy of simulated random processes. *Journal of Sound and Vibration* 1973; **26**(3): 417–428. DOI: 10.1016/S0022-460X(73)80196-8.
19. Bracewell R. *The Fourier Transform & Its Applications*, 3rd ed. McGraw-Hill Science/Engineering/Math: Boston,1999.
20. Newland DE. *An Introduction to Random Vibrations and Spectral Analysis*, 1st ed. Longman: London, 1975.
21. Wagner R, Antoniou I, Pedersen S, Courtney M, Jørgensen H. The influence of the wind speed profile on wind turbine performance measurements. *Wind Energy*; **12**(4): 348–362. DOI: 10.1002/we.297.
22. Antoniou I, Pedersen S, Enevoldsen P. Wind shear and uncertainties in power curve measurement and wind resources. *Wind Engineering* 2009; **33**(5): 449–468. DOI: 10.1260/030952409790291208.
23. Dolan D, Lehn P. Simulation model of wind turbine 3p torque oscillations due to wind shear and tower shadow. *IEEE Transactions on Energy Conversion* 2006; **21**(3): 717–724. DOI: 10.1109/TEC.2006.874211.
24. Sørensen P, Hansen A, Rosas P. Wind models for simulation of power fluctuations from wind farms. *Journal of Wind Engineering & Industrial Aerodynamics* 2002; **90**: 1381–1402. DOI: 10.1016/S0167-6105(02)00260-X.
25. Moreno C, Duarte H, Garcia J. Propagation of flicker in electric power networks due to wind energy conversion systems. *IEEE Transactions on Energy Conversion* 2002; **17**(2): 267–272. DOI: 10.1109/TEC.2002.1009479.
26. Apt J. The spectrum of power from wind turbines. *Journal of Power Sources* 2007; **169**(2): 369–374. DOI: 10.1016/j.jpowsour.2007.02.077.
27. Poulos G, Blumen W, Fritts D, Lundquist J, Sun J, Burns S, et al. CASES-99: a comprehensive investigation of the stable nocturnal boundary layer. *Bulletin of the American Meteorological Society* 2002; **83**(4): 555–581. DOI: 10.1175/1520-0477(2002)083<0555:CACIOT>2.3.CO;2.
28. Mahrt L, Vickers D. Boundary-layer adjustment over small-scale changes of surface heat flux. *Boundary-Layer Meteorology* 2005; **116**(2): 313–330. DOI: 10.1007/s10546-004-1669-z.

Wind Energ. 2012; **15**:699–715 © 2011 John Wiley & Sons, Ltd.
DOI: 10.1002/we

29. Maclean G, Oncley S. ATST site survey report. [cited 2010 Apr 21]; Available from: http://www.eol.ucar.edu/isf/projects/ATST/.
30. Socas-Navarro H, Beckers J, Brandt P, Briggs J, Brown T, Brown W, et al. Solar site survey for the advanced technology solar telescope. I. Analysis of the seeing Data. *Publications of the Astronomical Society of the Pacific* 2005; **117**(837): 1296–1305. DOI: 10.1086/496939.
31. Digital signal processing committee of the IEEE acoustics s and signal processing society. *IEEE Programs for Digital Signal Processing*. IEEE Press: New York, 1979.
32. Businger J. A note on the Businger-Dyer profiles. *Boundary-Layer Meteorology* 1988; **42**(1): 145–151.
33. Pasquill F. *Atmospheric Diffusion; The Dispersion of Windborne Material from Industrial and other Sources*, 1st ed. Van Nostrand: London, 1962.
34. Golder D. Relations among stability parameters in the surface layer. *Boundary-Layer Meteorology* 1972; **3**(1): 47–58.
35. Weber R. Remarks on the definition and estimation of friction velocity. *Boundary-Layer Meteorology* 1999; **93**(2): 197–209. DOI: 10.1023/A:1002043826623.
36. Iov F, Hansen A, Sørensen P, Blaabjerg F. Wind turbine blockset in MATLAB/Simulink. *Technical Report*, Aalborg University and the Risø DTU National Laboratory for Sustainable Energy: Roskilde, Denmark, March 2004. 1–108.
37. Hansen M, Hansen A, Larsen T, Øye S, Sørensen P, Fuglsang P. Control design for a pitch-regulated, variable speed wind turbine. In *Risø-R-1500(EN)*. Risø DTU National Laboratory for Sustainable Technology: Roskilde, Denmark, 2005; 1–84.
38. Sørensen P, Cutululis N, Vigueras-Rodríguez A, Jensen L, Hjerrild J, Donovan M, et al. Power fluctuations from large wind farms. *IEEE Transactions on Power Systems* 2007; **22**(3): 958–965. DOI: 10.1109/TPWRS.2007.901615.
39. Brower M. Development of eastern regional wind resource and wind plant output datasets, 2009. Available from: http://www.nrel.gov/wind/integrationdatasets/pdfs/eastern/2010/aws_truewind_final_report.pdf.
40. McGill R, Tukey J, Larsen W. Variations of box plots. *American Statistician* 1978; **32**(1): 12–16.